JOC Article

Improved Spin Trapping Properties by β-Cyclodextrin−Cyclic Nitrone Conjugate

Yongbin Han,[†,‡] Beatrice Tuccio,[§] Robert Lauricella,[§] and Frederick A. Villamena*[,†,‡]

Department of Pharmacology and Center for Biomedical EPR Spectroscopy and Imaging, The Davis Heart and Lung Research Institute, College of Medicine, The Ohio State University, Columbus, Ohio 43210, and Laboratoire Chimie Provence, UMR 6264, Equipe Spectrométries Appliquées à la Chimie Structurale, Case 512, Université de Provence-CNRS, Campus de Saint Jérôme, 13397 Marseille Cedex 20, France

frederick.villamena@osumc.edu

Received March 31, 2008

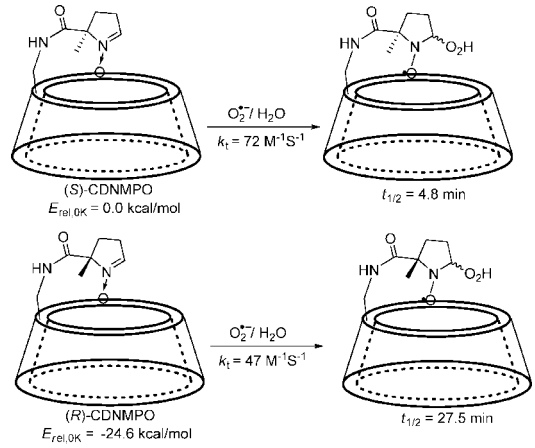

Spin trapping using a nitrone and electron paramagnetic resonance (EPR) spectroscopy is commonly employed in the identification of transient radicals in chemical and biological systems. There has also been a growing interest in the pharmacological activity of nitrones, and there is, therefore, a pressing need to develop nitrones with improved spin trapping properties and controlled delivery in cellular systems. The β-cyclodextrin (β-CD)−cyclic nitrone conjugate, 5-*N*-β-cyclodextrin-carboxamide-5-methyl-1-pyrroline *N*-oxide (CDNMPO) was synthesized and characterized. 1-D and 2-D NMR show two stereoisomeric forms (i.e., 5*S*- and 5*R*-) for CDNMPO. Spin trapping using CDNMPO shows distinctive EPR spectra for superoxide radical anion ($O_2^{\bullet-}$) compared to other biologically relevant free radicals. Kinetic analysis of $O_2^{\bullet-}$ adduct formation and decay using singular value decomposition and pseudoinverse deconvolution methods gave an average bimolecular rate constant of $k = 58 \pm 1$ M^{-1} s^{-1} and a maximum half-life of $t_{1/2} = 27.5$ min at pH 7.0. Molecular modeling was used to rationalize the long-range coupling between the nitrone and the β-CD, as well as the stability of the $O_2^{\bullet-}$ adducts. This study demonstrates how a computational approach can aid in the design of spin traps with a relatively high rate of reactivity to $O_2^{\bullet-}$, and how β-CD can improve adduct stability via intramolecular interaction with the $O_2^{\bullet-}$ adduct.

Introduction

Superoxide radical anion ($O_2^{\bullet-}$) has been shown to be the major precursor of some of the highly oxidizing species that are known to exist in biological systems, e.g., $ONOO^-$, $GSSG^{\bullet-}$, HOCl and $CO_3^{\bullet-}$. Reactive species including $O_2^{\bullet-}$ can cause oxidative damage to biomolecules resulting in loss of protein function, carbohydrate oxidation, DNA cleavage, or lipid peroxidation.[1] Oxidative damage to key biomolecular systems can lead to the pathogenesis of cardiovascular disease,[2] cancer,[3] inflammation,[4] or ischemia-reperfusion injury, to name a few.[5,6] Spin trapping is commonly used in the identification of free

[†] Department of Pharmacology.
[‡] Center for Biomedical EPR Spectroscopy and Imaging.
[§] Université de Provence-CNRS.

(1) Halliwell, B., Gutteridge, J. M. C. *Free Radicals in Biology and Medicine*; Oxford University Press: New York, 1999.
(2) Gutierrez, J.; Ballinger, S. W.; Darley-Usmar, V. M.; Landar, A. *Circ. Res.* **2006**, *99*, 924.
(3) Dreher, D.; Junod, A. F. *Eur. J. Cancer* **1996**, *32A*, 30.

10.1021/jo8007176 CCC: $40.75 © 2008 American Chemical Society
Published on Web 08/16/2008

SCHEME 1. Structures of 5*S*- and 5*R*-CDNMPO

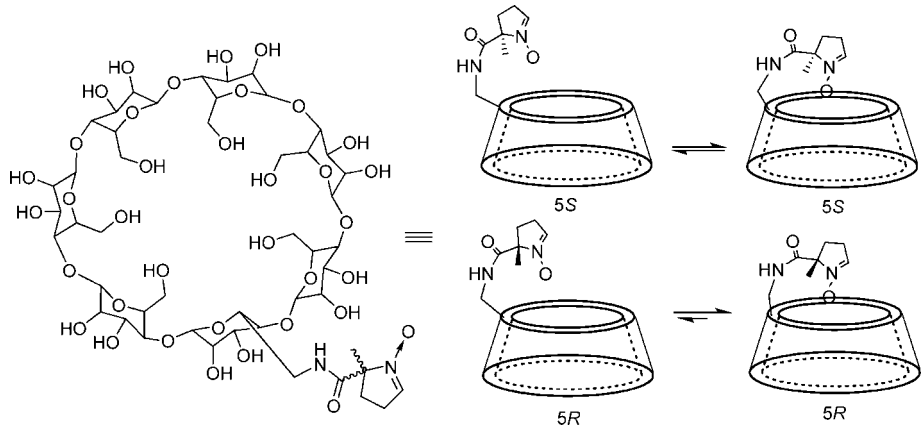

radicals in chemical and biological systems[7] and involves the addition of a short-lived radical to a nitrone spin trap, forming a persistent spin adduct that is detectable by electron paramagnetic resonance (EPR) spectroscopy.[7] The cyclic nitrones 5,5-dimethyl-1-pyrroline *N*-oxide (DMPO),[8] 5-ethoxycarbonyl-5-methyl-1-pyrroline *N*-oxide (EMPO)[9] and 5-diethoxyphosphoryl-5-methyl-1-pyrroline *N*-oxide (DEPMPO)[10] have been widely employed as spin traps but are still confronted by certain limitations such as slow reactivity to $O_2^{\bullet-}$ and low adduct stability.

Nitrones have also exhibited pharmacological activity such as in the treatment of neurodegenerative disease, acute stroke and cardioprotection from ischemia-reperfusion injury,[11−20] which paved the way toward the development of nitrones with improved spin trapping properties and controlled intracellular delivery. Efforts have been made to use methylated β-cyclodextrin (β-CD), either covalently[21] or noncovalently[22−26] bound to nitrones for improved spin-adduct stability. Moreover, we have previously shown that intramolecular H-bonding interaction plays a critical role in the stabilization of $O_2^{\bullet-}$ adduct,[27,28] and therefore, non-methylated β-CD may potentially exhibit a longer spin adduct half-life than the methylated ones. Although α-phenyl-*tert*-butyl nitrone (PBN) conjugate with methylated β-CD has been recently reported,[21] the non-methylated β-CD conjugate with cyclic nitrones has not been synthesized. Since cyclic nitrones have superior spin trapping properties compared to PBN and that non-methylated β-CD may exhibit extensive intramolecular H-bonding for improved adduct stability, it is important to explore the spin trapping properties of covalently bound cyclic nitrone with β-CD.

In this paper, we synthesized and characterized the β-CD−cyclic nitrone conjugate 5-*N*-β-cyclodextrin-5-carboxamide-5-methyl-1-pyrroline *N*-oxide (CDNMPO) (Scheme 1), and its spin trapping properties were investigated. Conformational studies of the nitrone and its radical adduct were carried out using NMR, circular dichroism, EPR and molecular modeling techniques.

Results and Discussion

Synthesis and Characterization. Our previous computational studies[29] show that substitution of pyrroline *N*-oxide at the C-5 position by *N*-methyl amide increases spin-trap reactivity to $O_2^{\bullet-}$. This increased reactivity was rationalized to be due to the polarization of $O_2^{\bullet-}$ spin density distribution resulting from the strong H-bond interaction between the amide N-H and $O_2^{\bullet-}$ in the transition state. Moreover, the use of *N*-monoalkylamide as linker group offers advantage over alkyl esters because amide bond is not susceptible to hydrolysis in the presence of intracellular esterases. We therefore synthesized CDNMPO by coupling racemic 5-carboxy-5-methyl-1-pyrroline *N*-oxide (CM-PO)[30] to 6-monodeoxy-6-monoamino-β-cyclodextrin (β-CD-NH_2)[31] via an amide bond using EDC/HOBt in DMSO. The resulting crude product was purified by precipitation using

(4) Petrone, W. F.; English, D. K.; Wong, K.; McCord, J. M. *Proc. Natl. Acad. Sci. U.S.A.* **1980**, *77*, 1159.
(5) Zweier, J. L.; Talukder, M. A. H. *Cardiovasc. Res.* **2006**, *70*, 181.
(6) Finkel, T.; Holbrook, N. J. *Nature* **2000**, *408*, 239.
(7) Villamena, F. A.; Zweier, J. L. *Antioxid. Redox Signaling* **2004**, *6*, 619.
(8) Finkelstein, E.; Rosen, G. M.; Rauckman, E. J. *J. Am. Chem. Soc.* **1980**, *102*, 4994.
(9) Olive, G.; Mercier, A.; Le Moigne, F.; Rockenbauer, A.; Tordo, P. *Free Radical Biol. Med.* **2000**, *28*, 403.
(10) Frejaville, C.; Karoui, H.; Tuccio, B.; Le Moigne, F.; Culcasi, M.; Pietri, S.; Lauricella, R.; Tordo, P. *J. Chem. Soc., Chem. Commun.* **1994**, 1793.
(11) Becker, D. A.; Ley, J. J.; Echegoyen, L.; Alvarado, R. *J. Am. Chem. Soc.* **2002**, *124*, 4678.
(12) Floyd, R. A. *Aging Cell* **2006**, *5*, 51.
(13) Ginsberg, M. D.; Becker, D. A.; Busto, R.; Belayev, A.; Zhang, Y.; Khoutorova, L.; Ley, J. J.; Zhao, W.; Belayev, L. *Ann. Neurol.* **2003**, *54*, 330.
(14) Nakae, D.; Kishida, H.; Enami, T.; Konishi, Y.; Hensley, K. L.; Floyd, R. A.; Kotake, Y. *Cancer Sci.* **2003**, *94*, 26.
(15) Nakae, D.; Uematsu, F.; Kishida, H.; Kusuoka, O.; Katsuda, S.-I.; Yoshida, M.; Takahashi, M.; Maekawa, A.; Denda, A.; Konishi, Y.; Kotake, Y.; Floyd, R. A. *Cancer Lett.* **2004**, *206*, 1.
(16) Floyd, R. A.; Hensley, K. *Ann. N.Y. Acad. Sci.* **2000**, *899*, 222.
(17) Packer, L.; Cadenas, E. *Handbook of Synthetic Antioxidants*; Marcel Dekker, Inc.: New York, 1997.
(18) Paracchini, L.; Jotti, A.; Bottiroli, G.; Prosperi, E.; Supino, R.; Piccinini, F. *Anticancer Res.* **1993**, *3*, 1607.
(19) von Frijtag, J. K.; Kunzel, D.; van der Zee, J.; Ijzerman, A. P. *Drug Dev. Res.* **1996**, *37*, 48.
(20) Zucchi, R.; Ghelardoni, S.; Evangelista, S. *Curr. Med. Chem.* **2007**, *14*, 1619.
(21) Bardelang, D.; Charles, L.; Finet, J.-P.; Jicsinszky, L.; Karoui, H.; Marque, S. R. A.; Monnier, V.; Rockenbauer, A.; Rosas, R.; Tordo, P. *Chem. Eur. J.* **2007**, *13*, 9344.
(22) Karoui, H.; Rockenbauer, A.; Pietri, S.; Tordo, P. *Chem. Commun.* **2002**, 3030.
(23) Kotake, Y.; Janzen, E. G. *J. Am. Chem. Soc.* **1992**, *114*, 2872.
(24) Karoui, H.; Tordo, P. *Tetrahedron Lett.* **2004**, *45*, 1043.
(25) Bardelang, D.; Rockenbauer, A.; Karoui, H.; Finet, J.-P.; Tordo, P. *J. Phys. Chem. B* **2005**, *109*, 10521.
(26) Bardelang, D.; Rockenbauer, A.; Karoui, H.; Finet, J.-P.; Biskupska, I.; Banaszak, K.; Tordo, P. *Org. Biomol. Chem.* **2006**, *4*, 2874.
(27) Villamena, F. A.; Hadad, C. M.; Zweier, J. L. *J. Am. Chem. Soc.* **2004**, *126*, 1816.
(28) Villamena, F. A.; Hadad, C. M.; Zweier, J. L. *J. Phys. Chem. A* **2005**, *109*, 1662.
(29) Villamena, F. A.; Xia, S.; Merle, J. K.; Lauricella, R.; Tuccio, B.; Hadad, C. M.; Zweier, J. L. *J. Am. Chem. Soc.* **2007**, *129*, 8177.
(30) Tsai, P.; Elas, M.; Parasca, A. D.; Barth, E. D.; Mailer, C.; Halpern, H. J.; Rosen, G. M. *J. Chem. Soc., Perkin Trans. 2* **2001**, 875.
(31) Zhong, N.; Byun, H.-S.; Bittman, R. *Tetrahedron Lett.* **1998**, *39*, 2919.

SCHEME 2. Structures of Compounds Used in This Study

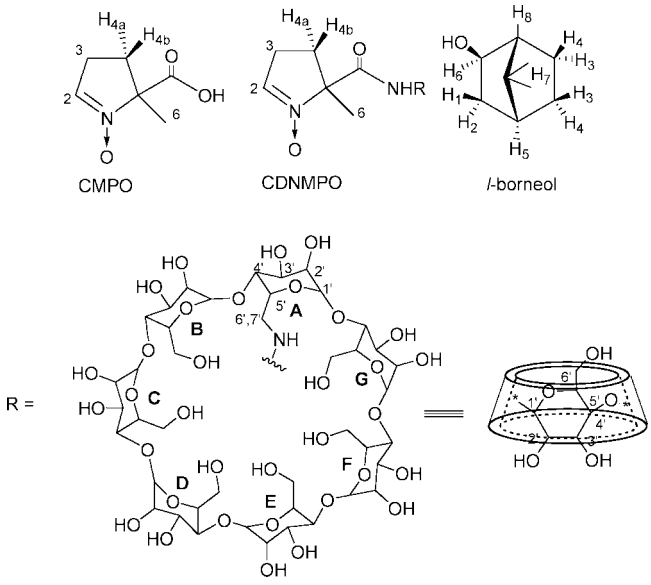

acetone followed by column chromatographic separation using Sephadex-C25 to remove the unreacted amino-β-CD. The product was further purified using reverse-phase (C18) preparative HPLC. The ^{1}H NMR, ^{13}C NMR, UV, IR and MS spectroscopic data (see Supporting Information) are consistent with the 5-*N*-β-cyclodextrin-carboxamide-5-methyl-1-pyrroline *N*-oxide (CDNMPO) structure.

NMR Studies. The formation of an association complex between a guest molecule and β-CD through hydrogen bonding or Van der Waals forces can lead to a highly chiral microenvironment around the guest nuclei.[32,33] Structural studies of CDNMPO were carried out using NMR spectroscopy, and the numbering system for CDNMPO and CMPO and the full assignments of their ^{1}H NMR spectra are shown in Scheme 2 and Figure 2, respectively, and are consistent to that previously reported.[34,35] Singlet peaks at 7.349 ppm and 1.588 ppm corresponding to $H_{CMPO}(2)$ and $H_{CMPO}(6)$, respectively, can be observed for the unconjugated CMPO (Figure 1a). Figure 1b shows two overlapping signals corresponding to the nitronyl hydrogen H(2) at 7.331 and 7.315 ppm of CDNMPO, while two nitrone methyl peaks appeared at 1.631 ppm and 1.616 ppm that will be assigned arbitrarily to the (5*S*)- and (5*R*)-CDNMPO isomers, respectively (see Scheme 1). From here on, the nitronyl hydrogen and methyl protons of (5*S*)- and (5*R*)-CDNMPO will be referred to as (5*S* or 5*R*)-H(2) and (5*S* or 5*R*)-H(6). No significant difference was observed in the H(3) and H(4) chemical shifts of CDNMPO compared to the unconjugated CMPO (see Figure S9 of Supporting Information). Furthermore, the ^{1}H NMR shifts of CDNMPO is not concentration-dependent within the range of 0.1−30 mM, indicating that the nitrone−β-CD interaction is intramolecular in nature (see Figure S4 of Supporting Information).[36] The two singlet peaks observed for H(2) and H(6) of CDNMPO have the same

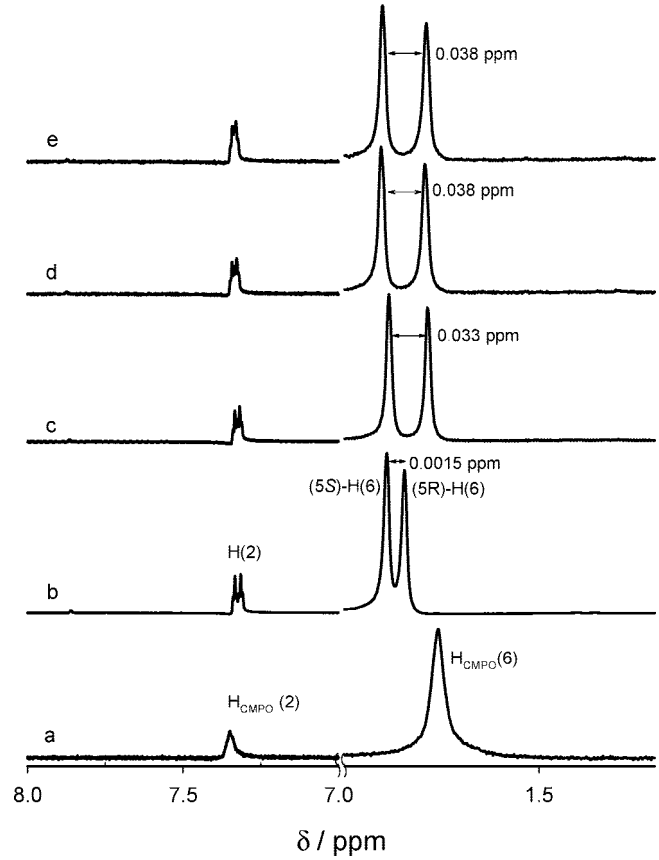

FIGURE 1. ^{1}H NMR chemical shifts of H(2) and (5*S* or 5*R*)-H(6) of (a) 5-carboxy-5-methyl-1-pyrroline *N*-oxide (CMPO), (b) CDNMPO, (c) CDNMPO with 0.5 equiv of *l*-borneol, (d) CDNMPO with 0.9 equiv of *l*-borneol, and (e) CDNMPO with 1.2 equiv of *l*-borneol in D_2O at 25 °C.

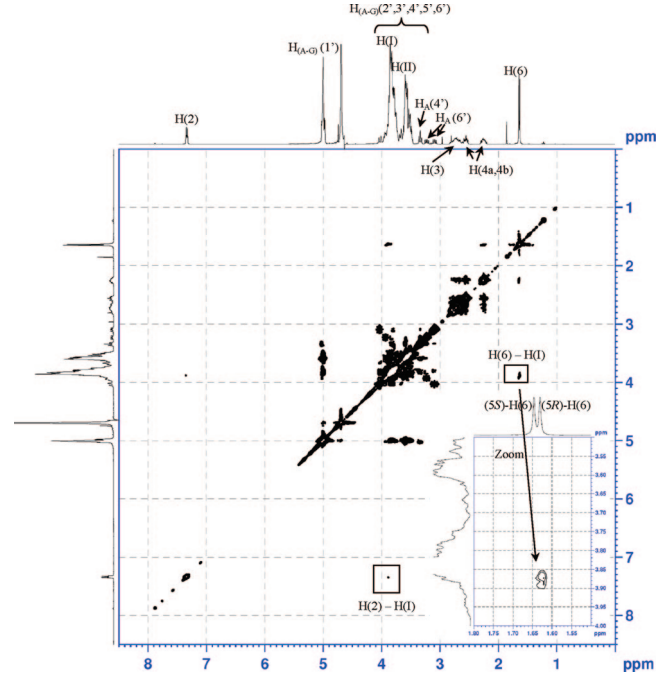

FIGURE 2. NOESY spectrum of CDNMPO in D_2O at 25 °C. Insert: expanded view of (5*S*)-H(6)−H(I) cross peak.

energy separation of $\Delta\delta$ = 0.015 ppm at 25 °C, while variable-temperature ^{1}H NMR at a temperature range of

(32) Schneider, H.-J.; Hacket, F.; Ruediger, V.; Ikeda, H. *Chem. Rev.* **1998**, *98*, 1755.
(33) Han, Y.; Cheng, K.; Simon, K. A.; Lan, Y.; Sejwal, P.; Luk, Y.-Y. *J. Am. Chem. Soc.* **2006**, *128*, 13913.
(34) Saka, W.; Yamamoto, Y.; Inoue, Y.; Chujo, R.; Takahashi, K.; Hattori, K. *Bull. Chem. Soc. Jpn.* **1990**, *63*, 3175.
(35) Stolze, K.; Udilova, N.; Rosenau, T.; Hofinger, A.; Nohl, H. *Biol. Chem.* **2003**, *384*, 493.

25−70 °C shows no significant change in $\Delta\delta$ with only a maximum of $\Delta\delta = 0.079$ ppm observed at 70 °C. This temperature dependence study demonstrates that the conformation of (5*R* or 5*S*)-CDMPO is relatively stable.[37,38]

The β-CD moiety of CDNMPO is composed of 7 glucopyranose units (i.e., A−G) and each unit has 7 protons, i.e., $H_A(1')$ to $H_A(7')$.[34] The overlapping signals at ∼3.8 and ∼3.6 ppm are due to $H_A(2'-7')$ to $H_G(2'-7')$ of the β-CD moiety and were generally assigned as H(I) and H (II), respectively. 2D-NMR nuclear Overhauser enhancement spectroscopy (NOESY) was used to investigate the through-space dipolar interaction between the protons of the nitrone moiety and that of the β-CD within 5 Å.[32] Figure 2 shows the NOESY spectrum of CDNMPO in D_2O at 25 °C, and two NOE correlations between the protons of the cyclic nitrone and β-CD moiety can be observed. The cross peaks between H(I) and the nitrone protons, H(2) and (5*S*)-H(6), indicate strong dipolar interaction between these nuclei, while H(3) and H(4) did not show NOE effect, indicating that these protons have weak interaction with the β-CD. Furthermore, the expanded view of the NOE correlation (see Figure 2 insert), which is further supported by molecular modeling as will be described below, reveals the correlation of the more upfield peak at 1.616 ppm corresponding to (5*R*)-H(6) with H(I), while the (5*S*)-H(6) did not show correlation with any of the β-CD protons. This data further suggest the presence of two stereoisomeric forms of CDNMPO in which the (5*S*)-CDNMPO isomer has the nitrone moiety exhibiting weak through-space interaction with the β-CD annulus, while the (5*R*)-CDNMPO isomer shows stronger interaction of H(2) and (5*R*)-H(6) with β-CD annulus, similar to the structural assignments shown in Scheme 1.

Molecular modeling was employed to further confirm the effect of stereoisomerism on the conformation of CDNMPO. The nitrone moiety was initially positioned on the β-CD annulus of (5*R*)- and (5*S*)-CDNMPO, and a conformational search using MMFF94[39] with GB/SA continuum solvation model[40] using water was performed (see Experimental Section for the computational details). The preferred conformations for (5*S*)- and (5*R*)-CDNMPO are shown in Figure 3 and show only a small difference on the location of the nitrone moiety relative to the β-CD annulus for (5*S*)- and (5*R*)-CDNMPO. The bottom-of-the-well energy difference at the HF/6-31G* level for the two isomers is ∼24.6 kcal/mol in which the *R* isomer is more stable than the *S* isomer. Further optimization of these two isomers at the HF/3-21G level shows that the *R* isomer is more embedded on the brim of the β-CD annulus compared to the *S* isomer (see Figure S10 in Supporting Information) with an energy difference of 10.7 kcal/mol at the HF/6-31G*//HF/3-21G level of theory with the *R* isomer also being more stable than the *S* isomer. However, the preferred conformations could not unequivocally identify which isomer exhibits the strongest through-space interaction between the protons as shown by the NOESY experiments since the methyl protons in both isomers are <5 Å away from the nearest β-CD-methylene protons. Conformational search also yields structures in which the methyl group directly points toward the annulus but are not energetically preferred. Therefore, it can only be reasonably assumed, on the basis of the relative energies of the two isomers, that through-space interaction in (5*R*)-CDNMPO is stronger than in the more labile (5*S*)-CDNMPO as the result of a more stable conformation of the former as shown in Scheme 1.

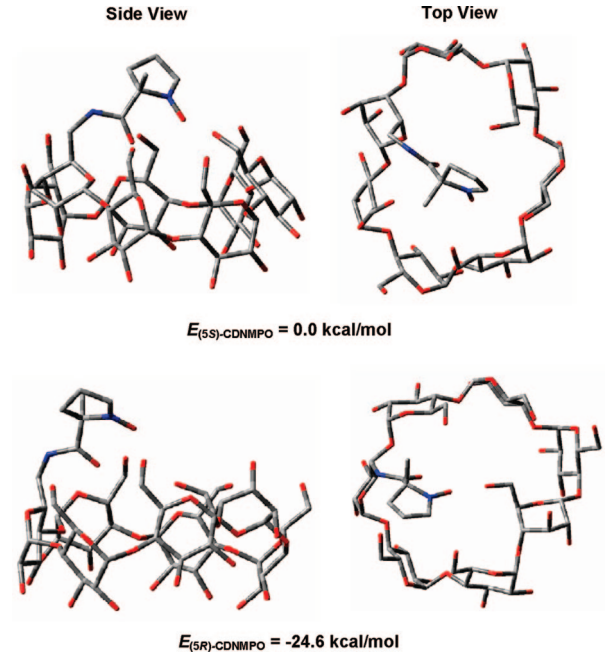

FIGURE 3. Lowest energy MMFF94 conformations in aqueous phase of (5*S*)-CDNMPO (top) and (5*R*)-CDNMPO (bottom). Values shown are bottom-of-the-well energies at the HF/6-31G* level. Atom labels: gray = carbon; red = oxygen; blue = nitrogen. The hydrogen atoms were omitted for clarity.

Inclusion Studies. The effect of a guest molecule, *l*-borneol, on the conformation of CDNMPO was also explored. *l*-Borneol has been extensively employed as a specific guest for the displacement of other guest molecules from β-CD.[41−43] Scheme 2 shows the chemical structure and numeral labeling of *l*-borneol. Although *l*-borneol is insoluble in water, it can be quantitatively solubilized in the presence of β-CD. Figure 1b−e shows the ^{1}H NMR spectra of 1.0 equiv of CDNMPO in the presence of 0, 0.5, 0.9, and 1.2 equiv of *l*-borneol. Only an upfield shift of the (5*S*)-H(6) signal (i.e., from 1.616 to 1.596 ppm) can be observed in the presence of an increasing amount of *l*-borneol. The peak separation between (5*R*)-H(6) and (5*S*)-H(6) increases as the amount of *l*-borneol is increased and reaches its maximum peak separation by 0.038 ppm at around 0.9 equiv of *l*-borneol. This study demonstrates that *l*-borneol can be included by β-CD and that the position of the cyclic nitrone on the β-CD annulus can be perturbed in the presence of a competitor guest molecule. The fact that only (5*R*)-H(6) is perturbed from the inclusion of *l*-borneol suggests that the configuration of one CDNMPO isomer has the nitrone methyl group being displaced by *l*-borneol from the annulus. However, only small perturbation on the H(2) chemical shift was observed in the presence of *l*-borneol, indicating that H(2) has weaker interaction than (5*R*)-H(6) with β-CD. On the other hand, there was no effect on the (5*S*)-H(6) chemical shift observed in the

(36) Ikeda, H.; Nakamura, M.; Ise, N.; Toda, F.; Ueno, A. *J. Org. Chem.* **1997**, *62*, 1411.
(37) Inoue, Y.; Miyauchi, M.; Nakajima, H.; Takashima, Y.; Yamaguchi, H.; Harada, A. *J. Am. Chem. Soc.* **2006**, *128*, 8994.
(38) Inoue, Y.; Miyauchi, M.; Nakajima, H.; Takashima, Y.; Yamaguchi, H.; Harada, A. *Macromolecules* **2007**, *40*, 3256.
(39) Halgren, T. A. *J. Comput. Chem.* **1996**, *17*, 490.
(40) Still, W. C.; Tempczyk, A.; Hawley, R. C.; Hendrickson, T. *J. Am. Chem. Soc.* **1990**, *112*, 6127.
(41) Liu, Y.; Zhang, Q.; Chen, Y. *J. Phys. Chem. B* **2007**, *111*, 12211.
(42) Yashima, E.; Maeda, K.; Sato, O. *J. Am. Chem. Soc.* **2001**, *123*, 8159.
(43) Ueno, A.; Ikeda, A.; Ikeda, H.; Ikeda, T.; Toda, F. *J. Org. Chem.* **1999**, *64*, 382.

SCHEME 3. Possible Conformations of CDNMPO in the Presence of *l*-Borneol

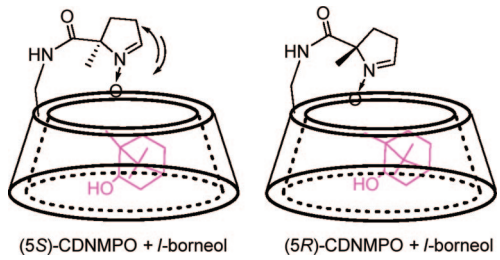

presence of *l*-borneol (Figure 1). This study is further supported by the calculated relative energies of (5*S*)- and (5*R*)-CDNMPO in which the former is more labile than the latter as shown in Scheme 3.

Examination of the NOESY spectrum of CDNMPO with 1.2 equiv of *l*-borneol (Figure 4) shows formation of an inclusion complex of both the nitrone moiety and the *l*-borneol guest with β-CD. Three correlation peaks were observed between *l*-borneol and β-CD, i.e., $H_{bor}(1,2)-H(I)$, $H_{bor}(5)-H(I)$, and $H_{bor}(8)-H(I)$, while the (5*R*)-H(6)−H(II) correlation peak can be observed for the nitrone and β-CD. Closer examination of the NOESY spectrum shows the existence of a correlation peak, (5*R*)-$H(6)-H_{bor}(8)$, indicating a strong interaction between the nitrone group and *l*-borneol in the β-CD annulus (see Figure S8 of Supporting Information). Interestingly, H(2)−H(I) correlation disappeared in the present of *l*-borneol, which indicates that *l*-borneol can perturb the H(2)-β-CD interaction. Also, the (5*R*)-H(6)−H(I) correlation was transformed to (5*R*)-H(6)−H(II) in the presence of *l*-borneol, which demonstrates that the position of the nitrone can be perturbed in the annulus in the presence other guest molecule.

Circular Dichroism Study. Molecular interaction between chiral (e.g., β-CD) and achiral (e.g., benzene) compounds can generate induced circular dichroism (ICD) of the achiral

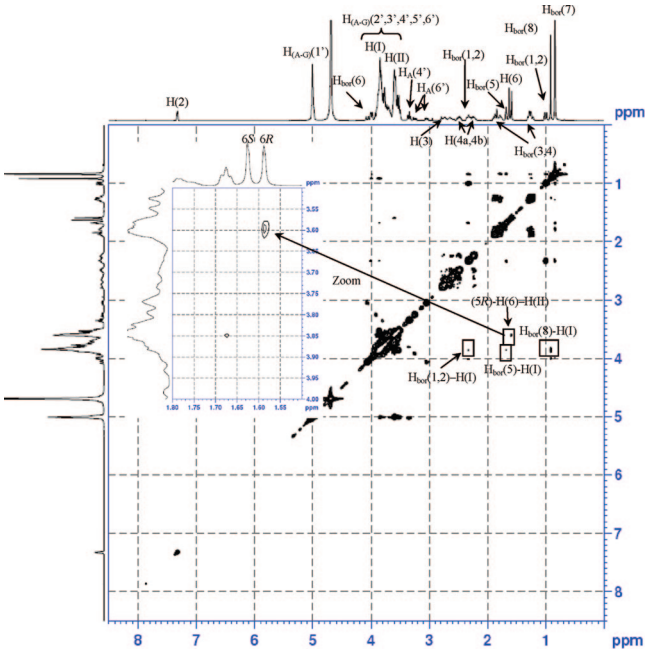

FIGURE 4. NOESY spectrum of CDNMPO in D_2O at 25 °C in the presence of 1.2 equiv of *l*-borneol. Inset: expanded view of the cross peak of (5*R*)-H(6)−H(II).

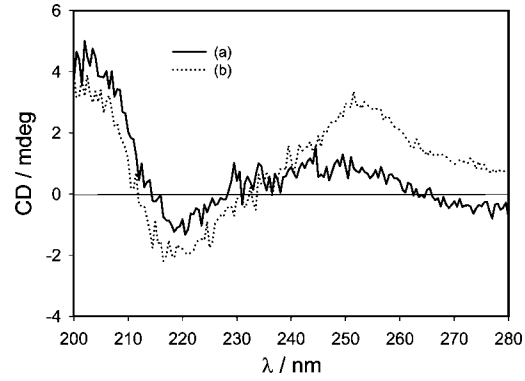

FIGURE 5. Circular dichroism of 20 mM CDNMPO (a) in the absence and (b) presence of 1.2 equiv of *l*-borneol in water at 25 °C. Cell pathway: 0.1 cm.

counterpart in the UV−vis region.[44] This spectroscopic technique has been extensively employed to explore the structural properties of inclusion complex not only of simple achiral molecules such as azobenzene,[45] xanthone and fluorenone,[46] ferrocene,[47] or naphtylethanol[48] but also of more complex chiral guests such as artemisinin,[49] suprofen[50] and ketoprofen.[51] However, there has been no reports on ICD studies involving nitrone as a guest molecule. In this work, we further investigated the interaction between the nitrone moiety and the annulus of the CDNMPO using ICD technique. Figure 5 shows the ICD spectra of CDNMPO between 200 to 280 nm in the presence and absence of *l*-borneol in water. CDNMPO (20 mM) shows a strong positive band at 203 nm and weak negative band at 218 nm (Figure 5a). These bands in the ICD spectrum of CDNMPO indicate interaction between the nitrone moiety and β-CD. However, in the presence of 1.2 equiv of *l*-borneol, the band at 243 nm due to CDNMPO alone exhibited a red shift to 251 nm with significant increase in intensity (Figure 5b), indicating perturbation of the nitrone conformation relative to β-CD by *l*-borneol. This observation further validates the NOESY studies mentioned above describing the complexation of β-CD with both *l*-borneol and the nitrone moiety, as well as the effect of *l*-borneol on the overall conformation of CDNMPO.

Spin Trapping Studies. (a) Superoxide Radical Anion. Superoxide radical anion ($O_2^{\bullet-}$) will be used to represent both superoxide and hydroperoxyl radicals since $O_2^{\bullet-}$ and its protonated form, $HO_2^{\bullet}$, lead to the same EPR-detectable spin adduct CDNMPO-O_2H as shown in Scheme 4. Figure 6 shows the experimental spectra and simulation traces of the CDNMPO-O_2H adducts from various $O_2^{\bullet-}$ generating systems. All of the EPR spectra gave the same spectral profile regardless of the $O_2^{\bullet-}$ generating system used. The highest field EPR line width (ΔB_{pp}) broadening is observed, which is indicative of short spin relaxation due to hindered molecular motion of the adduct from self-inclusion. No difference in ΔB_{pp} was observed at modula-

(44) Allenmark, S. *Chirality* **2003**, *15*, 409.
(45) Mayer, B.; Zhang, X.; Nau, W. M.; Marconi, G. *J. Am. Chem. Soc.* **2001**, *123*, 5240.
(46) Murphy, R. S.; Barros, T. C.; Barnes, J.; Mayer, B.; Marconi, G.; Bohne, C. *J. Phy. Chem. A* **1999**, *103*, 137.
(47) Harada, A.; Takahashi, S. *J. Inclusion Phenom.* **1984**, *2*, 791.
(48) Murphy, R. S.; Barros, T. C.; Mayer, B.; Marconi, G.; Bohne, C. *Langmuir* **2000**, *16*, 8780.
(49) Marconi, G.; Monti, S.; Manoli, F.; Degli Esposti, A.; Mayer, B. *Chem. Phys. Lett.* **2004**, *383*, 566.
(50) Sortino, S.; De Guidi, G.; Marconi, G.; Monti, S. *Photochem. Photobiol.* **1998**, *67*, 603.
(51) Monti, S.; Sortino, S.; De Guidi, G.; Marconi, G. *New J. Chem.* **1998**, *22*, 599.

SCHEME 4. Mechanism of Formation of CDNMPO-O_2H-a and CDNMPO-O_2H-b

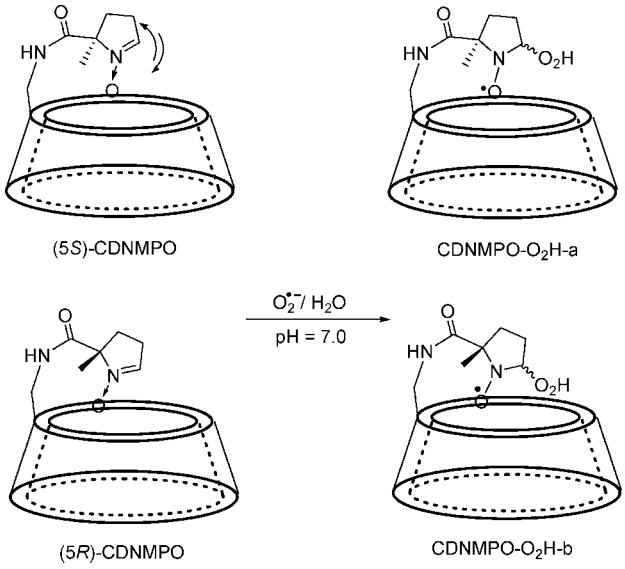

tion amplitudes of 0.5 and 1.2 G, indicating that the ΔB_{pp} broadening is due to the intrinsic spectral property of the adducts (see Figure S7 of Supporting Information).

On the basis of our previous studies,[28,29,52,53] chiral nitrones can give two diastereoisomeric $O_2^{\bullet-}$ adducts, i.e., *cis*- and *trans*-isomers, and their formation has been confirmed using EPR spectral simulation. Based on our NMR studies, CDNMPO has two configurational isomers, and therefore, four diastereoisomeric radical adducts can be formed. For simplicity, we only carried out EPR spectral simulation using two diastereomeric species. The difference of 0.8−1.2 G (Table 1) from the observed a_N between the *cis*−*trans* diastereomers of CDNMPO-O_2H is significantly higher compared to the observed difference in a_N between the *cis*−*trans* isomers of the HO_2-adducts of EMPO($\Delta a_{Ncis-trans}$ = 0.0 G),[9] AMPO ($\Delta a_{Ncis-trans}$ = 0.0 G),[54] BocMPO ($\Delta a_{Ncis-trans}$ = 0.1 G),[55] and DEPMPO ($\Delta a_{Ncis-trans}$ = 0.2 G).[56] This significant difference in the observed a_N for CDNMPO-O_2H isomers suggests that these two diastereomers (i.e., CDNMPO-O_2H-a and CDNMPO-O_2H-b) have distinct electronic properties due perhaps to their orientation relative to β-CD and may not exclusively be due to *cis or trans* isomerism. Bardelang et al.[25] reported that the nonincluded nitroxide has an a_N of 13.2 G but inclusion of the NO$^{\bullet}$ group to the β-CD cavity gave smaller nitrogen hyperfine coupling constant by 0.5−1.0 G. It can therefore be assumed that the 0.8−1.2 G difference from the a_N values of the CDNMPO-O_2H isomers is due to the position of the nitroxyl group relative to the β-CD (see Scheme 4). Moreover, careful analysis of the EPR spectrum of CDNMPO-O_2H shows no evidence of CDNMPO-OH formation even after 1 h of generating CDNMPO-O_2H, which suggests that the inclusion complex of HO_2-adduct prevents the unimolecular decomposition of the CDNMPO-O_2H to CDNMPO-OH, hence enhancing the $O_2^{\bullet-}$ adduct stability.

(52) Villamena, F. A.; Merle, J. K.; Hadad, C. M.; Zweier, J. L. *J. Phys. Chem. A* **2005**, *109*, 6083.
(53) Allouch, A.; Lauricella, R. P.; Tuccio, B. N. *Mol. Phys.* **2007**, *105*, 2017.
(54) Villamena, F. A.; Rockenbauer, A.; Gallucci, J.; Velayutham, M.; Hadad, C. M.; Zweier, J. L. *J. Org. Chem.* **2004**, *69*, 7994.
(55) Zhao, H.; Joseph, J.; Zhang, H.; Karoui, H.; Kalyanaraman, B. *Free Radical Biol. Med.* **2001**, *31*, 599.
(56) Frejaville, C.; Karoui, H.; Tuccio, B.; Moigne, F. L.; Culcasi, M.; Pietri, S.; Lauricella, R.; Tordo, P. *J. Med. Chem.* **1995**, *38*, 258.

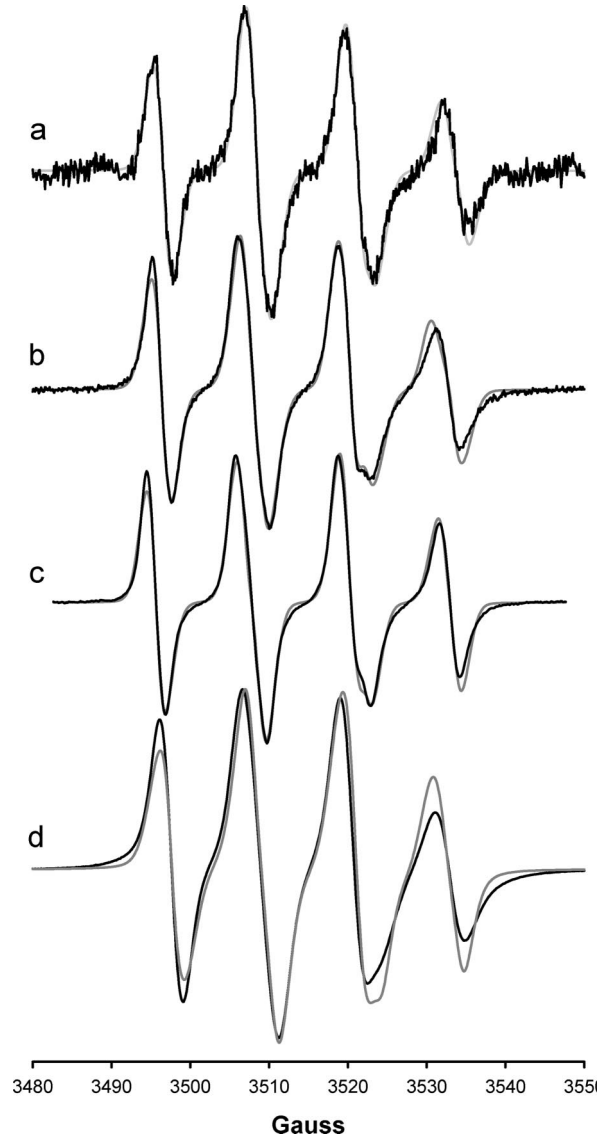

FIGURE 6. X-band EPR spectra of CDNMPO-O_2H generated from (a) light-riboflavin: a (49%) g = 2.00532, a_N = 13.2 G, $a_{\beta\text{-H}}$ = 11.4 G; b (51%) g = 2.00589, a_N = 12.4 G, $a_{\beta\text{-H}}$ = 11.4 G; (b) KO_2 in DMSO: a (68%) g = 2.00529, a_N = 13.1 G, $a_{\beta\text{-H}}$ = 10.9 G; b (32%) g = 2.00578, a_N = 12.0 G, $a_{\beta\text{-H}}$ = 10.9 G; (c) xanthine-xanthine oxidase: a (43%) g = 2.00582, a_N = 13.5 G, $a_{\beta\text{-H}}$ = 11.0 G; b (57%) g = 2.00554, a_N = 12.6 G, $a_{\beta\text{-H}}$ = 11.2 G; (d) H_2O_2 in pyridine: a (40%) g = 2.00555, a_N = 13.2 G, $a_{\beta\text{-H}}$ = 10.2 G; b (60%) g = 2.00572, a_N = 12.0 G, $a_{\beta\text{-H}}$ = 10.6 G. Simulated spectra are shown as trace plots.

TABLE 1. Relevant EPR Hyperfine Splitting Constants for the CDNMPO-O_2H Isomers Using Various Superoxide Radical Anion Generating Systems

	a_N (G)		Δa_N (G)	$a_{\beta\text{-H}}$ (G)		$\Delta a_{\beta\text{-H}}$ (G)
$O_2^{\bullet-}$ generating system	a	b	a_N(a) − a_N(b)	a	b	$a_{\beta\text{-H}}$(a) − $a_{\beta\text{-H}}$(b)
light/riboflavin	13.2	12.4	0.8	11.4	11.4	0
KO_2 in DMSO	13.1	12.0	1.1	10.9	10.9	0
X/XO	13.5	12.6	0.9	11.0	11.2	0.2
H_2O_2 in pyridine	13.2	12.0	1.2	10.2	10.6	0.4

(b) Hydroxyl and Other Radicals. Simulation of Figure 7a, d and e on the basis of only one species gave reasonable simulated results; however, Figure 7b, c and f require two

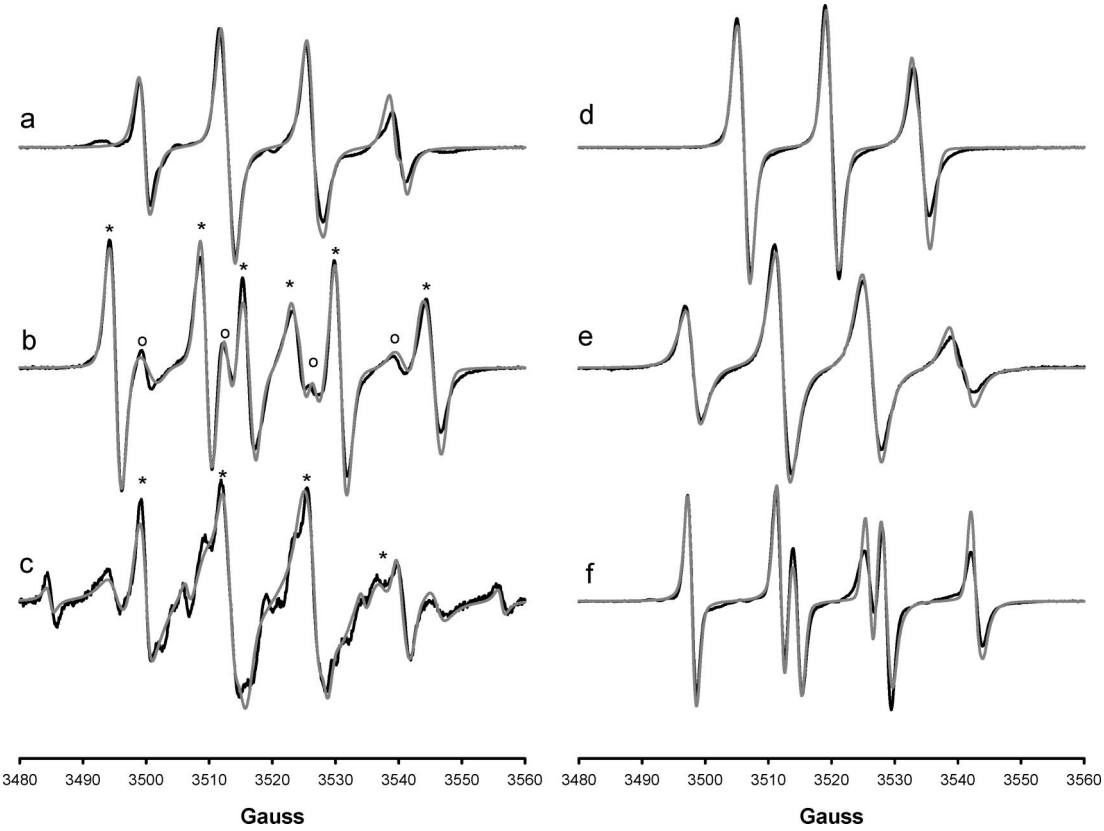

FIGURE 7. X-band EPR spectra of various radical adducts of CDNMPO. (a) hydroxyl radical: a (51%) $g = 2.00515$, $a_N = 14.2$ G, $a_{\beta\text{-H}} = 13.0$ G; b (49%) $g = 2.00546$, $a_N = 13.4$ G, $a_{\beta\text{-H}} = 12.5$ G; (b) α-hydroxyl-ethyl radical (marked by *): a (31%) $g = 2.00480$, $a_N = 14.9$ G, $a_{\beta\text{-H}} = 21.2$ G; b (40%) $g = 2.00497$, $a_N = 14.1$ G, $a_{\beta\text{-H}} = 21.6$ G; OH radical (marked by o) (29%); (c) *tert*-butoxy radical (marked by *): a (21%) $g = 2.00462$, $a_N = 13.2$ G, $a_{\beta\text{-H}} = 13.6$ G; b (34%) $g = 2.00496$, $a_N = 13.0$ G, $a_{\beta\text{-H}} = 10.4$ G; (d) sulfite radical: a (49%) $g = 2.00492$, $a_N = 14.3$ G; b (51%), $g = 2.00520$, $a_N = 13.3$ G; (e) glutathiyl radical: a (37%) $g = 2.00576$, $a_N = 13.5$ G, $a_{\beta\text{-H}} = 14.0$ G; b (63%) $g = 2.00531$, $a_N = 14.6$ G, $a_{\beta\text{-H}} = 14.5$ G; (f) carbon dioxide radical anion: a (37%) $g = 2.00512$, $a_N = 14.0$ G, $a_{\beta\text{-H}} = 16.7$ G; b (63%) $g = 2.00488$, $a_N = 15.9$ G, $a_{\beta\text{-H}} = 14.2$ G. Simulated spectra are shown as trace plots.

species for improved simulation. For consistency, all simulation was performed using two diastereoisomeric species.

Hydroxyl radical ($HO^{\bullet}$). The EPR spectrum of CDNMPO-OH (Figure 7a) was generated by UV photolysis of 0.2% H_2O_2 in the presence of CDNMPO (20 mM) in buffer solution. Simulation of the spectrum shows the presence of two diastereomeric adducts at 51%−49% ratio. The observed a_N and ΔB_{pp} for CDNMPO-OH are lower compared to CDNMPO-O_2H, making this spin trap suitable in discerning between $HO^{\bullet}$ and $O_2^{\bullet-}$.

α-*Hydroxyl-ethyl radical* ($CH_3C^{\bullet}HOH$). Two species of $CH_3C^{\bullet}HOH$ spin adducts at 31% and 40% ratio were observed (Figure 7b) and their hfsc values are typical of carbon centered radical adduct.[9]

tert-Butoxy radical (^{t}BuO$^{\bullet}$). ^{t}BuO$^{\bullet}$ was produced by UV photolysis of $(^t\text{BuO})_2$ giving a weak EPR signal of the CDNMPO-O^t*B*u adduct with significant amount of paramagnetic impurities (∼45%) (Figure 7c). This weak EPR signal is probably due to the bulky ^{t}BuO$^{\bullet}$ radical and crowded β-CD moiety making the ^{t}BuO$^{\bullet}$ addition to nitrone difficult.

Sulfite radical anion ($SO_3^{\bullet-}$). The CDNMPO-SO_3^- radical adduct (Figure 7d) gave only a triplet signal due to the nitrogen hyperfine splitting. Although the a_N of 14.3 and 13.3 G is similar to that expected for other CDNMPO spin adducts, the absence of a_H is quite intriguing. The same spectral profile was observed even after repeated experimentation and varying sulfite concentrations. We speculate that this phenomenon could be due to the a_H being equal or less than the ΔB_{pp}. We previously have shown that the formation of CPCOMPO-OSO_2^- and CP-COMPO-SO_3^- are both thermodynamically favored,[57] and it can therefore be assumed that the inclusion complex of the CDNMPO-OSO_2^- may result in the formation of a unique adduct conformation that allows hindered electron delocalization on the β-H. We have previously shown using density functional theory (DFT) approach[28] that the dihedral angle along the O−O−C−N bonds in DMPO-O_2H can significantly affect the spin density distribution on the β-H, and this phenomenon may also be true with CDNMPO-SO_3^- and therefore warrants further investigation.

Glutathiyl radical ($GS^{\bullet}$) and *carbon dioxide radical anion* ($CO_2^{\bullet-}$). Simulation of the EPR spectra of the CDNMPO-SG and CDNMPO-CO_2^- gave at least two diastereomeric adducts with relatively clean and distinctive EPR spectra. It is also interesting to note that $GS^{\bullet}$ was able to form an adduct with CDNMPO in spite of the bulky nature contrary to that observed for ^{t}BuO$^{\bullet}$ addition.

Determination of Rates of Formation and Decay of CDNMPO-O_2H. The kinetic method employed in this study has been previously described [58−60] with some modification in the rate law by considering two distinct adduct species. This

(57) Han, Y.; Tuccio, B.; Lauricella, R.; Rockenbauer, A.; Zweier, J. L.; Villamena, F. A. *J. Org. Chem.* **2008**, *73*, 2533.

(58) Allouch, A.; Roubaud, V.; Lauricella, R.; Bouteiller, J.-C.; Tuccio, B. *Org. Biomol. Chem.* **2005**, *3*, 2458.

SCHEME 5. Reactions 1−6 Considered in the Kinetic Model

$$X/XO \xrightarrow[k_x]{O_2} O_2^{\bullet-} \quad (1)$$

$$2\,O_2^{\bullet-} + 2\,H^+ \xrightarrow{k_{dis}} O_2 + H_2O_2 \quad (2)$$

$$O_2^{\bullet-} + (5S)\text{-CDNMPO} + H^+ \xrightarrow{k_{t,a}} \text{CDNMPO-O}_2\text{H-a} \quad (3)$$

$$O_2^{\bullet-} + (5R)\text{-CDNMPO} + H^+ \xrightarrow{k_{t,b}} \text{CDNMPO-O}_2\text{H-b} \quad (4)$$

$$(\text{CDNMPO-O}_2\text{H-a}) \xrightarrow{k_{d,a}} Y_1 \quad (5)$$

$$(\text{CDNMPO-O}_2\text{H-b}) \xrightarrow{k_{d,b}} Y_2 \quad (6)$$

SCHEME 6. Rate Equations 7−14 Considered in the Kinetic Model

$$d[X]/dt = -k_x[X] \quad (7)$$

$$d[O_2^{\bullet-}]/dt = k_x[X] - k_t[\text{CDNMPO}]\,[O_2^{\bullet-}] - 2k_{dis}[O_2^{\bullet-}]^2 \quad (8)$$

$$d[\text{CDNMPO-O}_2\text{H-a}]/dt = rk_t[(5S)\text{-CDNMPO}]\,[O_2^{\bullet-}] - k_{d,a}[\text{CDNMPO-O}_2\text{H-a}] \quad (9)$$

$$d[\text{CDNMPO-O}_2\text{H-b}]/dt = (1-r)k_t[(5R)\text{-CDNMPO}]\,[O_2^{\bullet-}] - k_{d,a}[\text{CDNMPO-O}_2\text{H-b}] \quad (10)$$

$$d[\text{CDNMPO}]/dt = -k_t[\text{CDNMPO}]\,[O_2^{\bullet-}] \quad (11)$$

$$[\text{CDNMPO}] = [(5S)\text{-CDNMPO}] + [(5R)\text{-CDNMPO}] \quad (12)$$

$$k_t = yk_{t,a} + (1-y)k_{t,b} \quad (13)$$

$$r = y\,k_{t,a}/k_t \quad (14)$$

modification was necessary because fitting of the experimental curves was unsuccessful without considering the formation of two spin adducts. The alternative model considered in this study is described by eqs 1−6 in Scheme 5, in which k_x is the rate constant for the superoxide formation; k_{dis} is the rate constant for the superoxide dismutation (at pH 7, $k_{dis} = 6.35 \times 10^5$ M^{-1} s^{-1}); k_t is the overall rate constant for the spin trapping reaction; y is the molar ratio of (5*S*)-CDNMPO; $k_{d,a}$ and $k_{d,b}$ are the rate constants for the decay of the two spin adducts, CDNMPO-O_2H-a and CDNMPO-O_2H-b, respectively; Y_1 and Y_2 are EPR silent species; r is the fraction of the spin trapping process that gives the nitroxide CDNMPO-O_2H-a. The rate eqs 7−14 given in Scheme 6 can be written based on the reactions described in Scheme 5. The two nitroxides CDNMPO-O_2H-a and CDNMPO-O_2H-b were not distinguishable in this approach, since their EPR spectra are very similar. The kinetic curve corresponds to the sum of the concentrations of both species (eq 15), and eq 16 was used to fit the experimental curve.

$$[\text{CDNMPO-O}_2\text{H}] = [\text{CDNMPO-O}_2\text{H-a}] + [\text{CDNMPO-O}_2\text{H-b}] \quad (15)$$

$$\frac{d[\text{CDNMPO-O}_2\text{H}]}{dt} = k_t[\text{CDNMPO}][O_2^{\bullet-}] - k_{d,a}[\text{CDNMPO-O}_2\text{H-a}] - k_{d,b}[\text{CDNMPO-O}_2\text{H-b}] \quad (16)$$

Figure 8 shows the formation and decay of CDNMPO-O_2H as a function of time after deconvolution of the experimental plots. Curve fitting of the four experimental plots yielded kinetic rate constants k_t, $k_{d,a}$, $k_{d,b}$, and r as shown in Table 2.

The experimental rate constant of 58 M^{-1} s^{-1} for CDNMPO is similar to that for CPCOMPO (60 M^{-1} s^{-1})[57] and higher compared to those of other nitrones, i.e., (in $M^{-1}s^{-1}$) DEPO

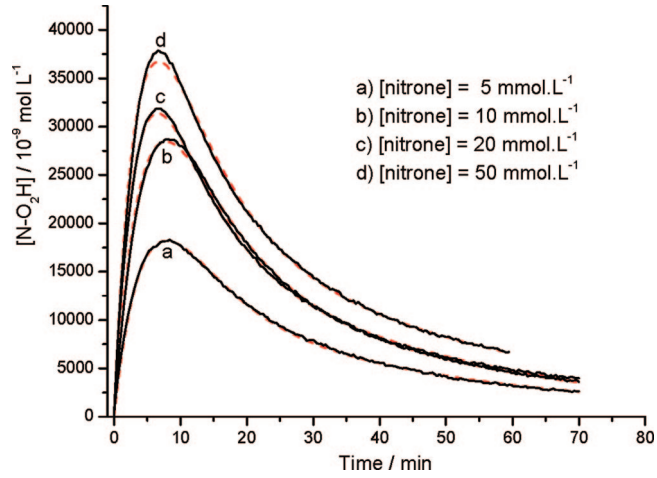

FIGURE 8. Experimental (black full lines) and calculated (red dotted lines) kinetic curves indicating the time-dependent changes in CDNMPO-O_2H concentration. The spin adduct was produced at pH 7.2 by generating superoxide in the presence of CDNMPO: (a) 5, (b) 10, (c) 20, and (d) 50 mM.

TABLE 2. Kinetic Parameters for CPCOMPO-O_2H Formation and Decay[a]

adduct	k_t[b]	k_d[c]	$t_{1/2}$	r
CDNMPO-O_2H-a	58 ± 1 M^{-1} s^{-1}	(2.4 ± 0.2) × 10^{-3} s^{-1}	4.8 min	0.65
CDNMPO-O_2H-b		(0.42 ± 0.04) × 10^{-3} s^{-1}	27.5 min	

[a] Using xanthine/xanthine oxidase radical generating system. [b] Using the y value of 0.52 obtained from the NMR spectra of CDNMPO (Figure 1), $k_{t,a}$ and $k_{t,b}$ can be calculated as 72 and 47 M^{-1} s^{-1}, respectively. [c] At CDNMPO concentration of 5−50 mM.

(31.1);[58] AMPO (25.2);[29] EMPO (10.9);[59] DEPMPO (3.95);[59] BocMPO (3.45);[58] DMPO (2.0).[60,61] Analysis of the kinetic curves allowed us to distinguish the two forms of spin trap that yield two different forms of spin adduct (for simplicity we only considered one diastereomeric adduct formed from each isomeric nitrone). The ^{1}H NMR spectra of the nitrone methyl group shown in Figure 1 yields a value of 0.52 for y. This permits us to individually calculate the rate constant of $O_2^{\bullet-}$ trapping by the two diastereoisomeric nitrones according to eqs 13 and 14 giving $k_{t,a}$ and $k_{t,b}$ values of ca. 72 and 47 M^{-1} s^{-1}, respectively. The spin adduct (5*S*)-CDNMPO has higher rate constant for adduct formation ($k_{t,a}$ = 72 M^{-1} s^{-1}) but with a shorter half-life of 4.8 min. Conversely, (5*R*)-CDNMPO gave a lower $k_{t,b}$ of 47 M^{-1} s^{-1} but longer half-life of 27.5 min. These differences in the rate of formation and half-lives could be mainly due to the position of the nitronyl carbon and the hydroperoxyl moiety, respectively, relative to the β-CD annulus. It is expected that the isomer in which the nitrone is more stabilized by the β-CD annulus will have a lower rate of spin trapping due to steric hindrance compared to when the nitrone moiety that is not stabilized by the β-CD where it is more accessible for radical addition. Moreover, the formation of an adduct in which the hydroperoxyl moiety is included inside the annulus is expected to give longer half-life due to its stabilization via H-bonding interaction with the β-CD. Kinetic analyses also show that the

(59) Lauricella, R.; Allouch, A.; Roubaud, V.; Bouteiller, J.-C.; Tuccio, B. *Org. Biomol. Chem.* **2004**, *2*, 1304.

(60) Lauricella, R. P.; Bouteiller, J.-C.; Tuccio, B. N. *Phys. Chem. Chem. Phys.* **2005**, *7*, 399.

(61) Allouch, A.; Roubaud, V.; Lauricella, R.; Bouteiller, J.-C.; Tuccio, B. *Org. Biomol. Chem.* **2003**, *1*, 593.

ratio of the two spin adducts is about 65/35 ($r = 0.65$) close to the ratio of 52/48 of the two nitrone methyl peaks as observed by ^{1}H NMR shown in Figure 1. Since the major diastereoisomer of the nitrone is not affected by addition of *l*-borneol on the basis of the NMR studies, we can therefore reasonably assume that the spin adduct CDNMPO-O_2H-a is derived from the major diastereoisomer (5*S*)-CDNMPO. These results show that the diastereoisomer with the most accessible nitrone function has the fastest rate of trapping $O_2^{\bullet-}$.

Longer half-life ($t_{1/2} = 28$ min) was observed for CDNMPO-O_2H-b compared to that reported for the $O_2^{\bullet-}$ adduct of DMPO in the presence of methylated β-CD in aqueous solution ($t_{1/2} = 6$ min).[22] It should be noted, however, that methylated β-CD and non-methylated CDNMPO could have significant difference in the nature of their respective host−guest interaction due to the absence of hydroxyl groups in the former. The noncovalent inclusion complex of methylated β-CD with PBN-O_2H gave a $t_{1/2}$ of 25 min,[24] close to the value observed for CDNMPO-O_2H-b, while the noncovalent inclusion complex of DEPMPO with methylated β-CD gave the longest half-life of $t_{1/2} = 96$ min[22] but using a kinetic model different to the one employed in this study.

Molecular Modeling of CDNMPO-O_2H. Intramolecular H-bonding interaction in $O_2^{\bullet-}$ adduct cyclic nitrones has been shown to play an important role in adduct stabilization.[27,28] In order to rationalize the extraordinary stability observed for CDNMPO-O_2H, their preferred conformations were computationally investigated. Figure 9 shows the various diastereomeric structures for CDNMPO-O_2H obtained from conformational searches by the MMFF94 method using the GB/SA continuum solvation model which showed no intramolecular H-bonding interaction. In all cases, the structures show projection of the N−O group toward the annulus due probably to Van der Waals interaction, which may be a significant factor to adduct stability. However, further optimization of these structures at the HF/3-21G level shows extensive H-bond interaction of the hydroxyl groups with the amide, hydroperoxyl and N−O groups (see Figure S11 of Supporting Information). Calculation of the bottom-of-the-well energies at the HF/6-31G*//MMFF94 level gave conformer (5*S*)-CDNMPO-O_2H-*trans* as the preferred isomer, whereas (5*R*)-CDNMPO-O_2H-*cis* is preferred at the HF/6-31G*//HF-3-21G level of theory.

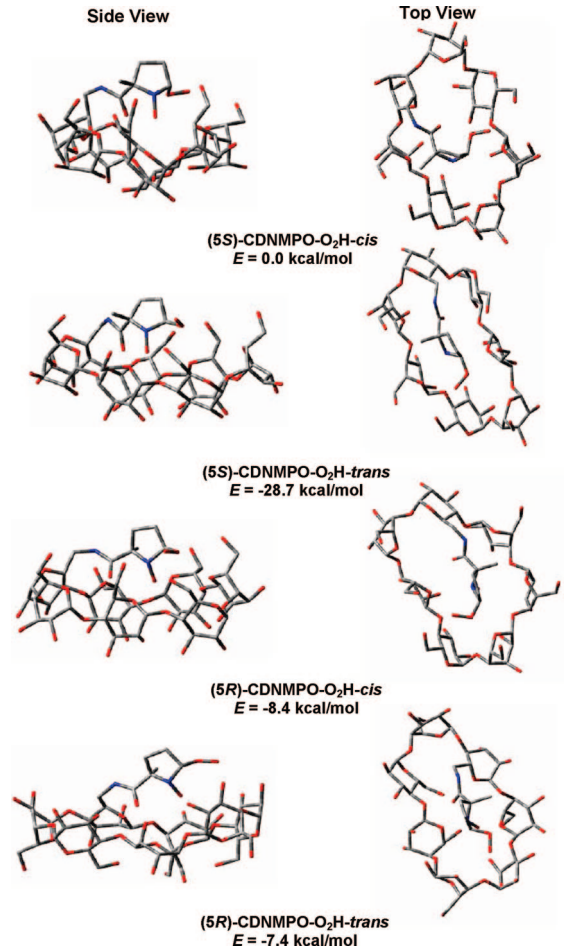

FIGURE 9. Lowest energy MMFF94 conformations in aqueous phase of CDNMPO-O_2H. Energies are bottom-of-the-well energies at the HF/6-31G* level. Atom labels: gray = carbon; red = oxygen; blue = nitrogen; white = hydrogen. The hydrogen atoms were omitted for clarity.

Conclusion

A cyclic nitrone conjugated to β-CD, CDNMPO, was synthesized and characterized. ^{1}H NMR, NOESY, molecular modeling, and ICD studies show the presence of two stereoisomeric forms for CDNMPO. The nitrone group in (5*R*)-CDNMPO exhibits stronger interaction with β-CD, whereas the nitrone group in (5*S*)-CDNMPO is more labile. The spin trapping properties of CDNMPO with various radicals was investigated and showed a distinctive EPR spectrum for each radical adducts, suggesting their suitability as spin trapping reagents. Spin trapping of $O_2^{\bullet-}$ gave diastereoisomeric adducts, and the rate constants for $O_2^{\bullet-}$ trapping by (5*S*)-CDNMPO and (5*R*)-CDNMPO adducts are 72 and 47 M^{-1} s^{-1}, respectively. The lower rate constant for (5*R*)-CDNMPO is attributed to steric hindrance upon $O_2^{\bullet-}$ addition. The overall rate constant for the CDNMPO-O_2H formation was relatively high ($k_t = 58$ M^{-1} s^{-1}) compared to the formation of DMPO, DEPMPO and EMPO $O_2^{\bullet-}$ adducts but comparable to that observed for CPCOMPO-O_2H (60 M^{-1} s^{-1}). The kinetics of (5*R*)-CDNMPO-O_2H decay shows an extraordinary longer half-life of $t_{1/2} = 28$ min compared to (5*S*)-CDNMPO-O_2H with $t_{1/2} = 5$ min due to stronger H-bond and Van der Waals interaction of the nitroxyl moiety of the *R* isomer with the β-CD annulus compared to the *S* isomer. This work demonstrates how theoretical studies and the inclusion phenomena can be exploited in the design of new spin traps with improved efficiency for $O_2^{\bullet-}$ trapping and longer adduct half-life.

Experimental Section

Synthesis of 5-*N*-β-Cyclodextrin-carboxamide-5-methyl-1-pyrroline *N*-Oxide (CDNMPO). A solution of mono-6-deoxy-6-amino-β-cyclodextrin (160 mg, 0.141 mmol), CMPO (40 mg, 0.282 mmol), EDC (64 mg, 0.338 mg), HOBt (19 mg, 0.141 mmol) and triethylamine (70 μL, 0.5 mmol) in 2 mL of DMSO was stirred under argon at ambient temperature for 2 days. Acetone was added to the reaction mixture to give the crude product as a precipitate. The precipitate was then dried in vacuo and purified by column chromatography using ion-exchange resin (NH_4^+ form) and water as eluent to afford the product as a gray solid. The product was then subjected to further purification using reverse-phase HPLC (C18 5 μm, 150 mm × 22 mm) using gradient elusion from 10% to 40% aqueous MeCN. Fractions were collected and solvents were removed in vacuo to afford the pure product CDNMPO as white powder (108 mg, 85% yield). ^{1}H NMR (400 MHz, D_2O, ppm): δ

1.60 (d, 3H), 2.18−2.22 (m, 1H), 2.49−2.56 (m, 1H), 2.68 (m, 2H), 3.30−3.93 (m, 42H), 4.99 (m, 7 H), 7.30 (m, 1H). ^{13}C NMR (250 MHz, D_2O, ppm): δ 21.3, 25.9, 31.2, 40.8, 60.3, 70.2, 70.4, 71.8, 72.0, 72.1, 73.1, 79.3, 80.5, 81.1, 83.2, 83.4, 101.4, 101.6, 101.9, 102.1, 145.4, 172.2. IR (neat, cm^{-1}) ν 3344, 2926, 2469, 1657, 1590, 1454, 1365, 1154, 1081, 1026, 966, 857, 750, 697. MALDI calcd for $C_{48}H_{78}N_2NaO_{36}$ ($M + Na^+$) *m/z* 1281.423, found 1281.350. UV (H_2O) $\lambda_{max} = 232$ nm, $\varepsilon = 960\ M^{-1}\ cm^{-1}$.

EPR Measurements. EPR measurements were carried out on an EPR spectrometer equipped with high sensitivity resonator at room temperature. Unless otherwise indicated, the instrument settings used for general spectral acquisition are microwave power, 20 mW; modulation amplitude, 1.2 G; receiver gains, 2×10^3–2×10^4; scan time 21 s; time constant, 41 s; sweep width, 80 G. All spin trapping studies were carried out in a phosphate buffer (PBS) (10 mM) at pH 7.0 containing 100 μM diethylene triamine pentaacetic acid (DTPA). Sample cells used were 50-μL quartz or glass capillary tubes for UV or non-UV irradiation experiments, respectively. EPR spectral simulation was carried out using the WINSIM[62] fitting program available as free software from Public Electron Paramagnetic Resonance Software Tools (http://epr.niehs.nih.gov).

Spin Trapping. (a) Superoxide radical anion. (*i*) *Light-riboflavin.* A 50 μL oxygenated PBS solution containing 0.1 mM riboflavin and 10 mM CDNMPO was irradiated with a 150-W light source positioned at 12 cm away from the sample cavity. (*ii*) *Xanthine-xanthine oxidase* (X-XO). A 50 μL PBS solution contains 100 μM DTPA, 0.4 mM xanthine, 0.5 unit/mL xanthine oxidase and 10 mM CDNMPO. (*iii*) *KO_2 generating system.* Superoxide adduct was generated by mixing 2.5 μL of 200 mM CDNMPO and 10 μL of 100 mM KO_2 in DMSO with 37.5 μL PBS buffer. (*iv*) *H_2O_2/pyridine system.* Pseudosuperoxide adduct was generated from 10 mM CDNMPO with 160 mM H_2O_2 in pyridine. **(b) Hydroxyl radical.** PBS solution containing 0.2% H_2O_2 and 20 mM CDNMPO was irradiated for 5 min using low-pressure mercury vapor lamp at 254 nm wavelength. **(c) Miscellaneous radicals.** Spin trapping of $SO_3^{\bullet-}$, $CO_2^{\bullet-}$, $CH_3^{\bullet}CHOH$, $GS^{\bullet}$ and $^tBuO^{\bullet}$ was carried out in 50 μL PBS solution containing 20 mM CDNMPO, 0.2% H_2O_2 and 100 mM of the respective radical source $NaHCO_2$, Na_2SO_3 and ethanol. $GS^{\bullet}$ and $^tBuO^{\bullet}$ was carried by UV photolysis of 100 mM GSSG and $(^tBuO)_2$. Each of the mixtures was irradiated with UV for a period of 5 min.

Determination of Rate Constants of CDNMPO-O_2H Formation and Decay. All kinetic measurements were carried out at pH 7 in 10 mM PBS using a X-XO superoxide generating system. In a typical experiment, the medium contains CDMPO (5, 10, 20 or 50 mM), 0.8 mM xanthine, 0.04 unit/mL xanthine oxidase and 3-carboxy-2,2,5,5-tetramethylpyrrolidin-1-oxyl (3-CP, 1.0 μM), as internal reference. The EPR spectrum was recorded 21 s after the initiation of radical production, and the succeeding spectra were recorded every 21 s for ca. 1 h. Noise reduction was accomplished using the singular value decomposition (SVD) procedure. The kinetic curves of the CDNMPO-O_2H adduct concentration as a function of time were obtained after deconvolution of the signal using the pseudoinverse method[59] which allows for the analysis of the formation of the CDNMPO-O_2H adduct alone from a series of EPR spectra without any contribution from any other paramagnetic species such as the OH adduct. These calculations were achieved using a homemade computer program written in FORTRAN, using subroutines given in Numerical Recipes.[63]

Curve fitting of the kinetic data was achieved using the homemade program Kalidaphnis (formerly Daphnis). The use of this program written in FORTRAN has been described in several papers[56,64] and it can be obtained upon request from the authors. It allows fitting of experimental curves as signal amplitude or concentration by numerical integration of appropriate rate equations. Application of the standard least-squares method yields pertinent kinetic parameters and their respective error values. Using this approach, the curves obtained at the three different initial concentrations of CDNMPO (5, 10, 20, 50 and 120 mM) were considered together and modeled using the rate equations shown in Scheme 6.

Computational Studies. All calculations were performed at the Ohio Supercomputer Center. The minimization of initial structures using MMFF94[39] were performed with MacroModel 9.6.[65] Conformational search was then carried out using MMFF94[39] via Monte Carlo Multiple Minimum method coupled with Generalized Born/Surface Area (GB/SA) continuum solvation model using water as the solvent[40] as implemented in the MacroModel package. The most preferred conformations for *R*- or *S*-CDMPO and the *cis/trans R*- or *S*-CDMPO-O_2H were based on the converged energies set at a threshold of 0.05 kcal/mol. The preferred geometries obtained from the first conformational search were further subjected to conformational search at least twice by employing the exact procedure mentioned above. The potential energies from all the combined conformational searches were sorted and the most favorable converged energy was chosen. Only in the case of *R*-CDMPO were two converged energies within ∼1 kcal/mol difference and therefore were both considered. The rest of the molecules gave second best energies which are at least ∼10 kcal/mol less favorable than the most preferred conformations, and therefore were not chosen. Bottom-of-the-well energies of the most preferred conformations were obtained from single point calculation using Hartree−Fock (HF) self-consistent field method[66] at the HF/6-31G* level of theory using Gaussian 03.[67] The Cartesian coordinates were generated using the GaussView 3.0 Program. Geometry optimization was also further carried out at the HF/3-21G level and bottom-of-the-well energies were obtained using single point calculation at the HF/6-31G* level.

Acknowledgment. This work is supported by NIH grant HL081248. The Ohio Supercomputer Center (OSC) is acknowledged for generous computational support of this research.

Supporting Information Available: Spectra and computational data. This material is available free of charge via the Internet at http://pubs.acs.org.

JO8007176

(62) Duling, D. R. *J. Magn. Reson., Ser. B* **1994**, *104*, 105.
(63) Press, W. H.; Teukolsky, S. A.; Vetterling, W. T.; Flannery, B. P. *Numerical Recipes in FORTRAN. The Art of Scientific Computing*, 2nd ed.; Cambridge University Press: Cambridge, 1992.
(64) Mathieu, C.; Tuccio, B.; Lauricella, R.; Mercier, A.; Tordo, P. *J. Chem. Soc. Perkin Trans.2* **1997**, 2501.
(65) *Macro Model*, 9.6 ed.; Schrödinger, LLC: New York, NY, 2005.
(66) Pople, J. A.; Nesbet, R. K. *J. Chem. Phys.* **1954**, *22*, 571.
(67) Frisch, M. J.; Trucks, G. W.; Schlegel, H. B.; Scuseria, G. E.; Robb, M. A.; Cheeseman, J. R.; Montgomery, J. A., Jr.; Vreven, T.; Kudin, K. N.; Burant, J. C.; Millam, J. M.; Iyengar, S. S.; Tomasi, J.; Barone, V.; Mennucci, B.; Cossi, M.; Scalmani, G.; Rega, N.; Petersson, G. A.; Nakatsuji, H.; Hada, M.; Ehara, M.; Toyota, K.; Fukuda, R.; Hasegawa, J.; Ishida, M.; Nakajima, T.; Honda, Y.; Kitao, O.; Nakai, H.; Klene, M.; Li, X.; Knox, J. E.; Hratchian, H. P.; Cross, J. B.; Bakken, V.; Adamo, C.; Jaramillo, J.; Gomperts, R.; Stratmann, R. E.; Yazyev, O.; Austin, A. J.; Cammi, R.; Pomelli, C.; Ochterski, J. W.; Ayala, P. Y.; Morokuma, K.; Voth, G. A.; Salvador, P.; Dannenberg, J. J.; Zakrzewski, V. G.; Dapprich, S.; Daniels, A. D.; Strain, M. C.; Farkas, O.; Malick, D. K.; Rabuck, A. D.; Raghavachari, K.; Foresman, J. B.; Ortiz, J. V.; Cui, Q.; Baboul, A. G.; Clifford, S.; Cioslowski, J.; Stefanov, B. B.; Liu, G.; Liashenko, A.; Piskorz, P.; Komaromi, I.; Martin, R. L.; Fox, D. J.; Keith, T.; Al-Laham, M. A.; Peng, C. Y.; Nanayakkara, A.; Challacombe, M.; Gill, P. M. W.; Johnson, B.; Chen, W.; Wong, M. W.; Gonzalez, C.; Pople, J. A. *Gaussian 03*; Gaussian, Inc.: Pittsburgh, PA, 2003.